Available online at www.sciencedirect.com

ScienceDirect

Procedia CIRP 79 (2019) 159–164

www.elsevier.com/locate/procedia

12th CIRP Conference on Intelligent Computation in Manufacturing Engineering, 18-20 July 2018, Gulf of Naples, Italy

# Real-time spatter detection in laser welding with beam oscillation

Martin Wilhelm Haubold[a,]*, Michael Friedrich Zäh[b]

[a]*Institute for Machine Tools and Industrial Management (iwb), Technical University of Munich, Boltzmannstraße 15, 85748 Garching, Germany*
[b]*Institute for Machine Tools and Industrial Management (iwb), Technical University of Munich, Boltzmannstraße 15, 85748 Garching, Germany*

* Corresponding author. Tel.: +49 89 289 15479; Fax: +49 89 289 15555. E-mail: martin.haubold@iwb.mw.tum.de

**Abstract**

Spatter formation is a longstanding issue in laser welding. This research addresses this topic and proposes a machine vision algorithm executed on a graphics processing unit to detect spatters in real time. Using this approach, a control system detecting spatter at a rate of 1 kHz and with a resolution of 900 x 900 *pixels* was implemented. Based on an experimental series, it is shown that the variation of the process parameters has a significant influence on the formation of spatter. It was also possible to quantify the variance of the spatter formation for a given set of process parameters.


Peer-review under responsibility of the scientific committee of the 12th CIRP Conference on Intelligent Computation in Manufacturing Engineering.

*Keywords:* laser welding; spatter formation; machine vision; beam oscillation; graphics processing unit

## 1. Introduction

Remote laser welding using scanner optics is becoming increasingly popular in industrial applications. The reasons for this include the fast and precise spot positioning, which reduces non-productive times, and the good accessibility of workpiece cavities [1]. The formation of spatter during the welding process is still a pressing issue for many industries. Especially for manufacturers of products with a high added value, it is necessary to provide documented proof of their quality standards. This is linked to the need for an automated control of all produced components regarding the resulting welding spatters. One possibility to implement such a monitoring system technically and economically is a so-called vision module for scanner optics. This makes it possible to observe the process zone coaxially to the laser beam. A process camera with a CMOS sensor is usually used for this purpose. For a fully functional monitoring system, not only the hardware, but also the appropriate software is required to automatically evaluate the images recorded by the camera. Within this work, the development of such a software is presented.

Experimental investigations are then described to determine the frequency of spattering for a variety of welding parameters. To additionally influence the weld seam, the used scanner optics are able to superimpose the feeding motion with an oscillatory beam movement, a so-called beam oscillation. The most common oscillation pattern of many commercial scanners is the circular oscillation, which is described by equation (1):

$$\begin{bmatrix} x \\ y \end{bmatrix} = \begin{bmatrix} v_w \cdot t + A \cdot sin(2 \cdot \pi \cdot f \cdot t + \pi/2) \\ A \cdot sin(2 \cdot \pi \cdot f \cdot t) \end{bmatrix} \quad (1)$$

The beam position at the x-coordinate is determined by the combination of the linear movement ($v_w \cdot t$) and the circular movement ($A \cdot sin(2 \cdot \pi \cdot f \cdot t + \pi/2)$). The linear component only depends on the welding speed $v_w$ and the process time $t$. The circular movement is defined by the oscillation amplitude $A$, the oscillation frequency $f$ and the process time $t$. For the calculation of the y-coordinate, only the circular component has an impact. The maximum oscillation frequency and amplitude are limited by the scanner's dynamics and the control system's performance [2]. In addition to $A$, $f$ and $v_w$, the experimental space to be investigated in this work regarding the formation of spatters is spanned by the laser power $P$.

2212-8271 
Peer-review under responsibility of the scientific committee of the 12th CIRP Conference on Intelligent Computation in Manufacturing Engineering.
10.1016/j.procir.2019.02.037

### 1.1. State of the Art

The following description of the state of the art is divided into three main parts. First, research activities concentrated on the underlying physics to spatter formation are discussed. Second, machine learning approaches to reduce spatter are presented. Finally, various process monitoring methods are outlined.

#### 1.1.1. Spatter Formation

The formation of spatters was studied by [3] and [4]. They stated different qualitative cause-effect chains and a categorization for the spatter phenomena reported in over 50 other research papers.

[5] used high-speed imaging and X-ray transmission imaging to investigate the spatter formation as well as the molten pool behavior. As a conclusion, the following three relationships between the spatter formation and the molten pool behavior were obtained; a higher laser power leads to a turbulent molten pool and thus increases spatter formation. The focal position has a major influence on the flow in the molten pool and thus determines the shape of spatter. When the focal position was inside the workpiece, a reduced spatter formation was reported.

The effect of a static magnetic field on the spatter formation was examined by [6]. They were able to observe that above a certain strength of the magnetic field, a stabilizing effect on the molten pool occurs. This reduces the number of spatters significantly.

Empirical and numerical studies on the effect of the process parameters on the spatter formation for aluminum alloys were carried out by [7]. They found that high welding speeds lead to more but smaller spatter. Also, full penetration welds tend to create less spatter than partial penetration welds.

[8] built a three-dimensional numerical model, which takes shear stresses and fluid mechanics into account, in order to investigate the reasons for spatter formation. As a result, they identified two main reasons why spatter form primarily around the keyhole. The surface tension of the molten metal around the keyhole is low and the recoil pressure caused by evaporation accelerates the upward moving melt around the keyhole.

Based on the model of [8], [9] used an advanced version to further investigate spatter formation. They concluded that spatter formation is significantly reduced if shear stresses around the keyhole are kept low.

#### 1.1.2. Machine Learning

To reduce spattering during laser welding, machine learning methods are also used.

[10] developed a neural network system to classify different welds according to the quality levels defined by the ISO 13919. By using images of cross sections to train the neural network, they developed a quality index based on the weights of the network and could classify welds into three levels of the EN-ISO standard.

To evaluate the welding status as a function of the bead width, [11] designed an artificial neural network. They used the size and number of spatters as well as the geometric features of the vapor plume as input variables. Experimental findings showed that a neural network trained by 15000 groups of plume and spatter characteristics can observe the welding status.

To implement a closed control loop for laser welding, [12] used a combination of a convolutional autoencoder and a support vector machine. The autoencoder extracts characteristic features from the images of the welding process. Based on these features, the support vector machine categorizes the current welding status according to the quality levels defined by the ISO 13919. As a result, it was possible to maintain a high welding quality by controlling the laser power.

#### 1.1.3. Process Monitoring

In addition to the investigations of the spatter formation mechanisms and the machine learning approaches to improve the welding quality, different process monitoring strategies have been examined. [13] reviewed over 50 research papers on this topic.

For the laser spot welding process with pulsed radiation, [14] developed a camera-based monitoring system. A high-speed camera took images coaxially through the beam path of a fixed-point optics. After evaluating the acquired images, the authors were able to measure the welding spot and to check for spatter formation during the welding process.

[15] extended the principal of the coaxial process monitoring to scanning optics. Using a field programmable gate array unit called Eye-RIS VS, the authors detected spatter occurrence by a segmentation algorithm during the welding process.

[16] presented two different methods for online and offline spatter detection. For the online image processing, they proposed a camera with an integrated processor per pixel processing unit. The offline algorithm utilized a Hough-transformation and separated overlapping spatters.

[17, 18 and 19] developed a spatter tracking algorithm to identify correlations between spattering and the visual weld seam quality. After recording high-speed image sequences of a high-power laser welding process, they concluded that the viscous friction drag of the energized vapor plume is the driving force for spatter formation at full penetration welding.

[20] used a different approach for a spatter tracking program by adapting a Kalman-filter. They used this program to monitor a laser welding process with beam oscillation. As a result, three different spatter formation mechanisms were distinguished.

In summary, it can be stated that up to now several methods for quantitative evaluation of the spatter behavior have been proposed, but the measurement systems were not able to detect spatter in real-time using standard computer hardware. The present work addresses this topic and investigates the variance of spatter formation for a laser welding process with beam oscillation.

### 1.2. Structure

The subsequent sections address the issue of a validated spatter detection algorithm from [21] and describe an advanced version as well as a data processing algorithm for real-time

spatter evaluation. Therefore, the experimental set-up (see section 2) including the necessary computer hardware is described in detail at first. Section 3 includes the data processing algorithm and the modifications to the image processing. In section 4 the monitoring system is used to draw conclusions on the robustness of parameter combinations based on the variance of spatter formation. A conclusion with a summary of the described algorithms and an outlook towards future work concerning spatter reduction are given in section 5.

## 2. Experimental set-up

For the experimental study, the welding optics elephant50 by ARGES was used. It featured a spot diameter of $d_f = 50.5\ \mu m$, which was measured with a Primes Micro Spot Monitor. It was also equipped with a vision module for observing the process zone coaxially to the laser beam. The resulting 3 *cm* x 3 *cm* field of view was monitored by a process camera (EoSens 3CXP) with a monochrome CMOS sensor.

To ensure the detection of small and fast spatters by the process camera, a temporal resolution of 1000 $Hz$ and a spatial resolution of 900 *pixels* x 900 *pixels* was chosen. These settings allow the robust identification of spatter at speeds up to 10 $m/s$ and a minimum diameter of 50 $\mu m$. The image processing operations were carried out on a NVIDIA P5000 with 16 GB GDDR5X memory. The CPU used for the data processing and program management was an AMD Ryzen 7 1700x. During the experiments, the specimens of the oxygen-free copper CW008A were only partially penetrated by the laser beam. The laser source was an ytterbium-doped YAG single mode (SM) fiber laser by IPG Photonics. It emits a continuous wave (cw) radiation with a maximum output power of $P_{max} = 3\ kW$ at a wavelength of $\lambda = 1070\ nm$.

## 3. Method for real-time spatter detection

The proposed method for detecting spatters at a frame rate of 1000 $Hz$ and a resolution of 900 *pixels* x 900 *pixels* consists of two independent algorithms. The data processing algorithm ensures a real-time execution of the program, while the image processing algorithm segments the spatters in the high-speed images. The following section describes the structure and sequence of the data processing algorithm. Subsequently, the development of the image processing algorithm will be discussed in more detail.

### *3.1. Data processing*

The data processing algorithm is based on the consumer-producer design pattern; however, it contains several modifications. Every implementation of the consumer-producer design pattern consists of the producer which provides the data, the queue which handles the data and the consumer which evaluates the data. Fig. 1 shows the procedure of the version implemented in this work.

The frame grabber, which transfers the images from the camera directly to the GPU memory, represents the producer in this scenario. The queue is implemented as a class and organizes the access rights to its elements. Each element of the queue is an instance of the *queue element* class, which consists of the image data itself and a time stamp as fields of the class. The consumer contains the image processing source code, which is executed on the GPU and yields the spatter number and size for the evaluated image.

A multithreaded approach is used to execute the operations needed by the producer, the queue, and the consumer. The only instance of the producer runs in a single thread and is therefore independent of the other components. There is also only a single instance of the queue, which runs in a separate thread. Because the execution time of one consumer is generally longer than 1 $ms$, multiple instances calculating in parallel are needed to ensure real-time computation. The exact computation time of a single consumer thread varies depending on the number of occurring spatters in an image. Therefore, in this work 100 consumer threads are launched when the program starts. All consumers are in an idle state until an image is copied into the queue. Every time an unprocessed image arrives, the queue activates a consumer instance, which executes the image processing algorithm. After completion, the consumer deletes the image data from the GPU memory and saves the spatter number and the spatter size to the main memory. Another implementation of the queue class is used for storing the image processing results. This guarantees that all consumer instances can store the results without violating access rights in the main memory. Hence, the evaluation is strongly parallelized and is only limited by the memory space on the GPU. The maximum number of images that can be processed in parallel is thus determined by the ratio of the memory requirements of an image and the available memory space of the GPU.

The following section describes the procedure of the image processing algorithm, which runs in every consumer thread, in more detail.

### *3.2. Image Processing*

To ensure a fast computation of the image processing, the algorithm is divided into two parts. The first part is completed offline and before the process monitoring. The second part is real-time capable and executed within the consumer threads. The calculations for a background model, a process mask, and a global threshold value using computationally intensive and non-parallel image processing operations is done in the first part of the algorithm. This requires a reference welding experiment, which only needs to be repeated if the optical system is changed, e. g. if the protective glass is replaced.

Fig. 3 illustrates the offline part of the image processing algorithm. After the reference experiment has been carried out, all recorded images are averaged by their grayscale value. For calculating the process mask, the images are weighted equally. The resulting averaged image is binarized using Otsu's method. Because Otsu's method is based on a separation of the image foreground from the background by evaluating the histogram, only the bright process zone will be left as foreground. The next step implements a morphological dilation to slightly increase the size of the process mask. The resulting image can be used to block out the process zone, which would cause many false spatter detections.

For calculating a precise background model, which reproduces the noise caused by the optical components without

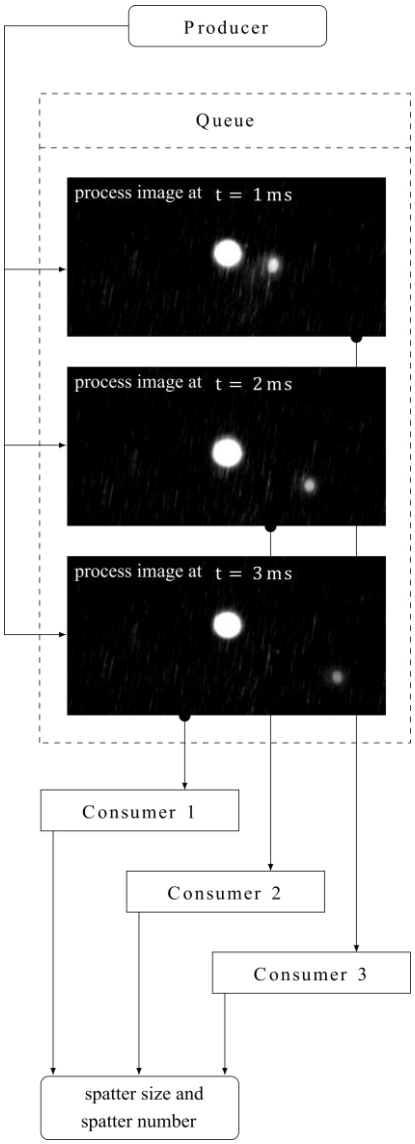


Fig. 1: Data processing algorithm following the producer-consumer design pattern

occurring spatter, the recorded images are weighted and averaged. The weighting factors are calculated by the structural similarity (SSIM) index, which uses an image without any spatter as a reference. This way, images with spatters are weighted weaker than images without spatter. Lastly, to calculate the background model, a contrast limited adaptive histogram equalization (CLAHE) is performed to enhance the contrast of the image.

To compute a global threshold value, the process mask is subtracted from the background model. Subsequently, the threshold value is calculated by Otus's method. Since the bright process zone is no longer a factor for the calculation of the threshold, a suitable value for the segmentation of the spatters is determined.

Based on the background model, the process mask, and the global threshold value, the spatter segmentation algorithm runs in each consumer thread. The calculation of the spatter number and the spatter size is carried out by subtracting the process mask and the background model from the input image. The resulting image shows the spatters as regions in the foreground of the image. After applying the global threshold value, the spatter number is determined by counting the connected components in the black and white image. The size of each spatter is defined as the number of white pixels in the connected component.

For the following experimental investigations, both the number of spatters occurring per image and the mean size of the spatters are evaluated. Both variables have already been used by [22] to provide information about the welding quality with the help of a dimensionless number. The quality vector $\vec{Q}$ shown in equation (2) stores the spatter size and number for each image and is evaluated in the following section.

$$\vec{Q} = \begin{bmatrix} n_{spat} \\ mean(A_{spat}) \end{bmatrix} \tag{2}$$

## 4. Experimental Findings

Using the monitoring system, the tendency for spatters within the design space from Table 1 was investigated experimentally. Four parameter combinations were selected, all of which led to the welding of two copper sheets with a thickness of 1 mm each. There was no penetration welding present. Each parameter combination was welded ten times and the corresponding quality vector was recorded.

Fig. 4 shows the spatial progression of the averaged value of the spatter number and the mean spatter size for the four parameter combinations.

Table 1: Design space used for the experimental investigations

| Welding parameter | minimum value | maximum value |
|---|---|---|
| welding velocity $v_w$ in $mm/s$ | 20 | 100 |
| oscillation amplitude $A$ in $mm$ | 0.05 | 1.0 |
| oscillation frequency $f$ in $Hz$ | 10 | 300 |
| laser power $P$ in $W$ | 300 | 3000 |

Each trend line of the spatter number was calculated by averaging over the ten repetitions. Before determining the trend lines for the spatter size in the same way, the mean value of the spatter size was computed for each image.

The graph concerning the spatter number shows the two parameter combinations #1 and #2 with a consistently low number of occurring spatters, which correlated with a high seam quality. Parameter combination #3 leads to a higher spatter formation compared to #1 and #2. In addition, an oscillatory character of the trend line is apparent.

The overall highest amount of spatter occurs with parameter combination #4. An increased spatter formation at the beginning of the weld seam is visible. This can be explained by an unsteady piercing process.

The trend lines of the spatter numbers show variations, which can be correlated with the resulting quality of the weld seams.

For the parameter combination #4, a correlation between the size and the number of spatters is observed. Each peak in the trend line of the spatter number also has a corresponding peak in the spatter size graph. However, this characteristic does not apply to the other parameter combinations. Especially with parameter combination #3, the spatters are generally small.

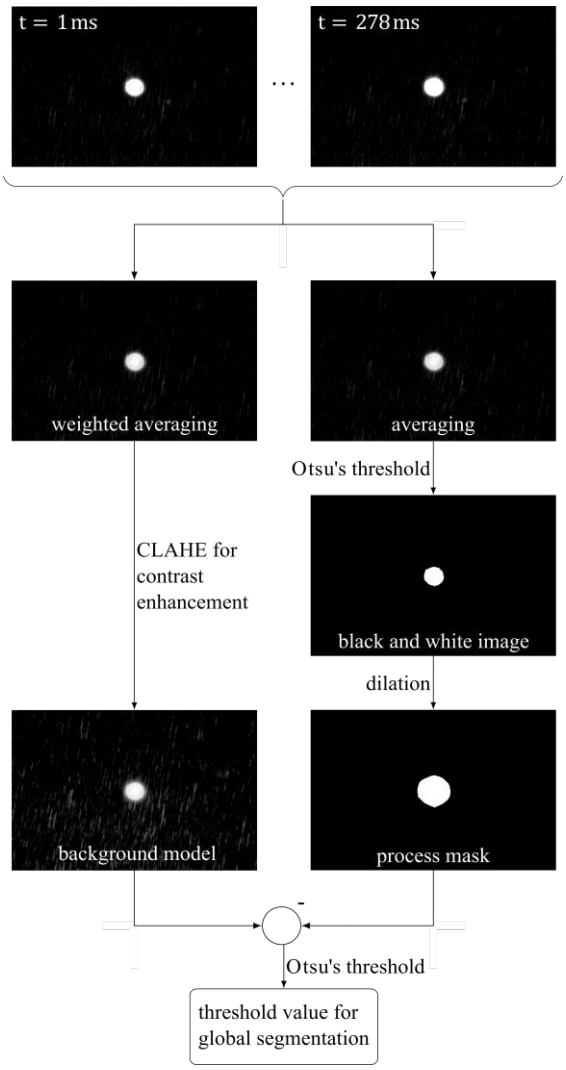


Fig 3: Image processing algorithm for calculating a background model, a process mask and a global threshold value

The low trend lines of the spatter size for parameter combinations #1 and #2 c explained by the fact that only sporadic spatters occur. Depending on the application, either the spatter number or the spatter size can be used as a quality criterion.

Table 2: Mean value and standard deviation of the spatter number after ten repetitions

| # | $v_w$ in $mm/s$ | $A$ in $mm$ | $f$ in $Hz$ | $P$ in $W$ | Mean value of the spatter number | Standard deviation of the spatter number |
|---|---|---|---|---|---|---|
| 1 | 30.00 | 0.47 | 242.0 | 1929 | 0.04 | 0.07 |
| 2 | 51.25 | 0.81 | 173.3 | 2287 | 0.02 | 0.03 |
| 3 | 71.50 | 0.44 | 74.0 | 1980 | 0.57 | 0.77 |
| 4 | 50.00 | 0.15 | 150.0 | 1800 | 1.61 | 1.37 |

To investigate the reproducibility of spatter formation, the mean values and the standard deviation were calculated for ten repetitions. The results for the spatter number and for the spatter size are shown in Table 2 and in Table 3 respectively.

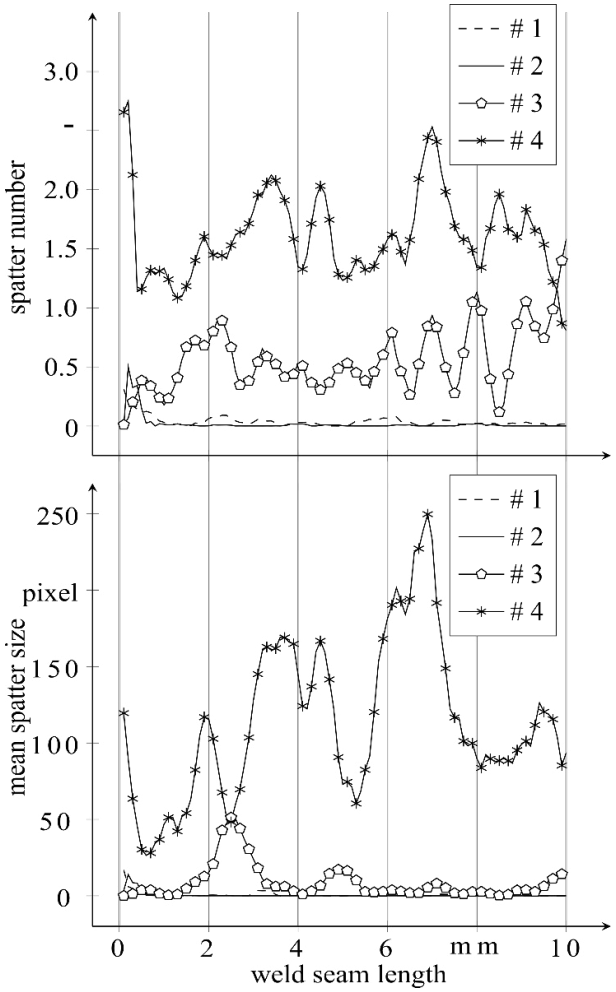


Fig 4: Trend lines of the spatter number and the mean spatter size averaged over ten repetitions along the weld seam length

For the parameter combination #1, with an average value of 0.04, spatters over the length of the weld seam occur only sporadically. Since the standard deviation takes a comparatively small value as well, a stable and repeatable process result was observed. The same is true for the parameter combination #2; only slightly fewer spatters occur.

The parameter combination #3 shows a clearly increased spatter number. The mean value and the standard deviation for the spatter number are in the same order of magnitude as for the parameter combinations #1 and #2. This trend also continues for the parameter combination #4. Since the parameter combination #4 has an even higher spatter number than #3, it can be concluded that the variance for spatter formation increases with a rising number of spatters. In addition, it can be stated that by using beam oscillation the amount of spatter can be influenced significantly. Although parameter combination #4 has the lowest laser power and the same welding speed as #2, the spatter formation is significantly increased. The interactions of all four process parameters must be considered to ensure a welding process with few spatters.

Table 3 shows that the spatter size varies significantly more than the spatter number over the ten repetitions. The standard deviation for each parameter combination is higher than the corresponding mean value. This indicates that it is considerably more difficult to influence the spatter size than the spatter number. The parameter combinations #1 and #2 are

characterized by a small spatter number as well as a small spatter size. This correlates in both cases with a high weld seam quality.

Table 3: Mean value and standard deviation of the spatter size after ten repetitions

| # | $v_w$ in $mm/s$ | $A$ in $mm$ | $f$ in $Hz$ | $P$ in $W$ | Mean value of the spatter size | Standard deviation of the spatter size |
|---|---|---|---|---|---|---|
| 1 | 30.00 | 0.47 | 242.0 | 1929 | 0.70 | 1.98 |
| 2 | 51.25 | 0.81 | 173.3 | 2287 | 0.40 | 0.41 |
| 3 | 71.50 | 0.44 | 74.0 | 1980 | 8.56 | 20.17 |
| 4 | 50.00 | 0.15 | 150.0 | 1800 | 114.00 | 162.06 |

The experiments show that the parameter combinations #1 and #2 repeatedly produce weld seams with a high quality.

## 5. Conclusion and Outlook

This paper presented an algorithm for real time spatter detection at $1000\,Hz$ using commercial hardware. This was achieved by splitting the algorithm into a data processing part and an image processing part. Both components of the algorithm run in parallel and thus allow a high evaluation speed.

The resulting monitoring system was used to investigate the reproducibility of spatter formation during remote laser beam welding with beam oscillation. The results show significant differences in the spatter number and spatter size for varying process parameters. This indicates that beam oscillation is suitable for reducing spatter formation. The investigations also showed a clear correlation between the spatter number and the corresponding standard deviation. This means that a parameter combination that results in fewer spatter is more robust and repeatable at the same time. The standard deviation of the spatter size was larger than the corresponding mean value for all examined parameter combinations. The repeatability of the spatter size is therefore not given.

In future work, the monitoring system will be used to develop an algorithm for systematic spatter reduction, thus, finding welding parameters that lead to a high seam quality.

## 6. Acknowledgements

The project, on which this report is based, was funded by the Federal Ministry of Education and Research under the funding label 13N13916. The authors are responsible for the content of this publication.

## References

[1] Zaeh MF, Moesl J, Musiol J, Oefele F. 2010. Material Processing with Remote Technology - Revolution or Evolution?, in: 6th Laser Assisted Net Shape Engineering (LANE). Erlangen, 09/21 – 09/24/2010, pp. 19 – 33.

[2] Pieczona SJ, Zollitsch S, Zaeh MF. 2017. Dynamics enhancement of galvanometer laser scanners by adaptive inverse control, in: IEEE International Conference on Advanced Intelligent Mechatronics (AIM). Munich, 07/03 – 07/07/2017, pp. 253 – 258.

[3] Kaplan A, Powell J. 2010. Laser welding: The spatter map, in: International Congress on Applications of Lasers & Electro-Optics. Tucson, 09/26 – 09/30/2010, pp. 683 – 690.

[4] Kaplan A, Powell J. Spatter in laser welding. Journal of Laser Applications (2011); 23 pp. 1 7.

[5] Li S, Chen G, Katayama S, Zhang Y. Relationship between spatter formation and dynamic molten pool during high-power deep-penetration laser welding. Applied Surface Science, (2014) 303 pp. 481 – 488.

[6] Rong Y, Xu J, Cao H, Zheng H, Huang Y, Zhang G. Influence of steady magnetic field on dynamic behavior mechanism in full penetration laser beam welding. Journal of Manufacturing Processes, 19 (2017) 3 pp. 399 – 406.

[7] Chang B, Blackburn J, Allen C, Hilton P. Studies on the spatter behaviour when welding AA5083 with a Yb-fibre laser. The International Journal of Advanced Manufacturing Technology, (2016) 12 pp. 1769 – 1776.

[8] Wu D, Hua X, Li F, Huang L. Understanding of spatter formation in fiber laser welding of 5083 aluminum alloy. International Journal of Heat and Mass Transfer, 113 (2017) pp. 730 – 740.

[9] Zhang D, Li C, Liu X, Cao Y, Wu D. Numerical study of spatter formation during fiber laser welding of aluminum alloy. Journal of Manufacturing Processes, 31 (2018) pp. 72 – 79.

[10] Galantucci LM, Tricarico L, Spina R. A Quality Evaluation Method for Laser Welding of Al Alloys Through Neural Networks. CIRP Annals, (2000) 1 pp. 131 – 134.

[11] Gao X, Sun Y, Katayama S. Neural network of plume and spatter for monitoring high-power disk laser welding. International Journal of Precision Engineering and Manufacturing-Green Technology, 1 (2014) 4 pp. 293 – 298.

[12] Günther J, Pilarski PM, Helfrich G, Shen H, Diepold K. Intelligent laser welding through representation, prediction, and control learning: An architecture with deep neural networks and reinforcement learning. Journal of Mechatronics, 34 (2015) 11 pp. 1 – 11.

[13] Purtonen T, Kalliosaari A, Salminen A. Monitoring and Adaptive Control of Laser Processes. Physics Procedia, 56 (2014) pp. 1218 – 1231.

[14] Stache NC, Zimmer H, Gedicke J, Olowinsky A, Aach T. Robust High-Speed Melt Pool Measurements for Laser Welding with Sputter Detection Capability. Pattern Recognition, (2007) 4713 pp. 476 – 485.

[15] Nicolosi L, Tetzlaff R, Felix A, Andreas H, Blug A, Höfler H. 2012. Novel algorithm for the real time multi-feature detection in laser beam welding. IEEE International Symposium on Circuits and Systems, pp. 181 – 184.

[16] Lahdenoja O, Säntti T, Laiho M, Poikonen J. Spatter Tracking in Laser- and Manual Arc Welding with Sensor-level Pre-processing, in:, 22nd International Conference in Central Europeon Computer Graphics, (2014) 6 pp. 27 – 32.

[17] Zhang MJ, Chen GY, Zhou Y, Li SC, Deng H. Observation of spatter formation mechanisms in high-power fiber laser welding of thick plate. Applied Surface Science, 280 (2013) pp. 868 – 875.

[18] You D, Gao X, Katayama S. Monitoring of high-power laser welding using high-speed photographing and image processing. Mechanical Systems and Signal Processing, 49 (2013) 2 pp. 39 - 52

[19] You D, Gao X, Katayama S. Visual-based spatter detection during high-power disk laser welding. Optics and Lasers in Engineering, 54 (2014) pp. 1 – 7.

[20] Schweier M, Haubold MW, Zaeh MF. Analysis of spatters in laser welding with beam oscillation: A machine vision approach. CIRP Journal of Manufacturing Science and Technology, 14 (2016) pp. 35 – 42.

[21] Haubold MW, Wulf L, Zaeh MF. Validation of a spatter detection algorithm for remote laser welding applications. Journal of Laser Applications, 29 (2017) 2 pp. 1 10.

[22] Bidanda B, Rubinovitz J, Raman S. Development of a spatter index for automated welding inspection using computer vision. Computers & Industrial Engineering, 16 (1989) 2 pp. 215 – 224.